

Supplementary Information for

The subpolar gyre regulates silicate concentrations in the North Atlantic

H. Hátún, J. Ólafsson, K. Azetsu-Scott, R. Somavilla, F. Rey, C. Johnson,
M. Mathis, U. Mikolajewicz, P. Coupel, J-É. Tremblay, S. Hartman, S.V. Pacariz and I. Salter.

correspondence to: hjalmarh@hav.fo

This PDF file includes:

1. Materials and Methods
2. Supplementary Text
3. Supplementary Figs. S1 to S7

30 1. Materials and Methods

31

32 Silicate observations (see also Methods in the main manuscript)

33

34 The silicate observations reported here are from several independent hydrographic
35 sections crossing the Atlantic Inflow branches as well as the potential Arctic and subtropical
36 water mass sources (Fig. 1). The individual *primary datasets* have been sampled in a
37 consistent way and should be regarded as reliable. These are from the Labrador Sea (L in
38 Fig.1), the Irminger Sea (Ir) and the Nordic Seas (S,M,G), all shown with colored squares in
39 Fig. 1, and plotted in Fig. 2a. *Supporting datasets* are also utilized to support the primary
40 datasets and to investigate the causes for the marked silicate decline. These are from the
41 Iceland Basin (Ic), the Faroe Shelf (F), the Labrador Shelf (LC), the Porcupine Abyssal Plain
42 (P) and the Bay of Biscay (B), shown with the black circles in Fig. 1

43 Data were obtained from: the Bedford Institute for Oceanography (BIO), Canada, the
44 Marine Research Institute (MRI), Iceland, the Scottish Association for Marine Science
45 (SAMS), UK, the Faroe Marine Research Institute (FAMRI), Faroe Islands, the Institute of
46 Marine Research (IMR), Norway, the National Oceanography Centre (NOC), UK, and from
47 the Spanish Institute of Oceanography (IEO). Below we provide further details to the
48 Methods section in the main text.

49

50 Table S1 Overview over the silicate datasets

Location	Supplier	Depth (m)	Month	Comment
Labrador Sea (L)	BIO	150-500	May	Primary
Irminger Sea (Ir)	MRI	0-50	Feb-March	Primary
Nordic Seas (S,M,G)	IMR	0-200	March	Primary
Iceland Basin (Ic)	SAMS	150-600	Summer (varies)	Supporting
Faroe Shelf (F)	FAMRI	18	Dec-Feb	Supporting
Labrador Shelf (LC)	BIO	Hydr. criterion	May	Supporting
Porcupine Abyssal Plain (P)	NOC	Surface	March	Supporting
Bay of Biscay (B)	IEO	150 and 400	Every month	Supporting

51

52 In the central *Labrador Sea* (L, Fig. 1 and Table S1), all deep stations along the WOCE
53 line ARW7, referenced in the Fisheries and Oceans Canada (DFO) BioChem oceanographic
54 database (55.75-59.50°N, 53.50-49.50°W) were averaged from 150-500 m. The silicate
55 concentrations were determined at the BIO using a Technicon Autoanalyzer II characterized
56 by a 0.1 μM detection limit.

57 The *Irminger Sea* (Ir in Fig. 1 and Table S1) samples (64.33°N, 27.95°W) were
58 analyzed for dissolved silicate with standard so-called colorimetric methods, and the long
59 term accuracy has been estimated to $\pm 0.2 \mu\text{M}$. Details of the analytical methods and quality
60 assurance can be found in (ref. 42).

61 For the *Nordic Seas* observation sites (S, M and G, Fig. 1 and Table S1), samples were
62 taken in the upper mixed layer. This is defined as the shallowest of either the upper 200 m, or
63 the depths where the water density difference is less than 0.05 relative to the surface value¹⁴.
64 Samples were only taken in Atlantic Water, identified by salinities greater than 35 and
65 temperatures above 2°C.

66 The *Iceland Basin* (Ic in Fig. 1 and Table S1) time-series was calculated by averaging all
67 silicate samples from four stations along the 20°W portion of the Extended Ellett Line (EEL)
68 - latitude range 61.50 – 62.33°N (Fig. 4). Details of the analytical methods can be found in

69 (ref. 18). The EEL cruises are usually during the summer, but not at the same time each year.
70 A station-wise rate of change analysis reveals an increasingly negative trend towards Iceland
71 (Fig. S1)

72 For the *Faroe Shelf* (F in Fig. 1 and Table S1), the coastal station (Skopun, 61.91°N,
73 6.89°W) pumps water from 18 m depth and silicate samples have been collected twice a
74 week since 1995. The nutrient samples were preserved with 12 drops of chloroform per 100
75 ml of seawater in polyethylene bottles and measured 3-6 months later according to (ref. 43).

76 Data for the *Canadian Arctic Archipelago passages* (Lancaster Sound, Smith Sound and
77 Hudson strait, Fig. S6) come from the annual Arctic Net cruises (1998-2013) conducted on-
78 board the icebreaker Amundsen between July and October each year. The sampling and
79 analysis of the silicate concentrations were performed at University Laval according to the
80 method described in (ref. 8). Data prior to 1998 come from the ICES Data Centre
81 (<http://ices.dk/>).

82 For the *Labrador Shelf* (LC, Fig. 1 and Table S1), the silicate concentrations have been
83 averaged over the depth layer 50 -150 m, to avoid the impact of near-surface biological
84 activity (Fig. 5).

85 The *Porcupine Abyssal Plain* (PAP, P in Fig. 1 and Table S1) sustained observatory site
86 is described in (ref. 44). For comparisons with sensors at the site, surface nutrient data was
87 collected from a ship of opportunity on the UK-Caribbean route⁴⁵. This data set was sub
88 sampled for the region 45-52°N, 26.08-8.92°W to be close to the PAP site. On the UK-
89 Caribbean ship of opportunity route samples were collected and frozen on-board each month
90 for analysis ashore using a Skalar auto-analyser⁴⁶. Working standards were compared with
91 standards prepared by Ocean Scientific International (OSI) to ensure the results were
92 consistent from month to month. The precision obtained was assessed through duplicate
93 measurements as 0.1%.

94 For the southern *Bay of Biscay* (B in Fig. 1 and Table S1), silicate concentrations at the
95 northern station of the Santander standard section (150 m, 43.80°N, 3.78°W, 2580 m bottom
96 depth) is representative of the winter silicate concentration in the mixed layer (Fig. 3). The
97 samples for silicate were frozen and subsequently concentrations determined with a
98 Technicon autoanalyzer. For comparison these are plotted together with the near-surface
99 winter (March) silicate concentrations around the PAP mooring (see above) (Fig. 3).

100
101 Ocean model description (see also Methods in the main manuscript)

102
103 The primitive equations of oceanic motion in the MPIOM are discretized on an Arakawa
104 C-grid with z-coordinates and free surface, including hydrostatic and Boussinesq
105 approximations. Tracer and momentum advection follows a second order total variation
106 diminishing scheme after (ref. 47). Vertical mixing is performed after (ref. 48) with an
107 additional parameterization for wind stirring³⁹. In the model version described here, the full
108 ephemeridic luni-solar tidal potential is included according to (ref. 49). A detailed model
109 description and evaluation is given in (refs. 50,51). For the specific application to the
110 northern North Atlantic region, a stretched grid configuration has been used with non-
111 diametrical poles located in southwest Germany and Wisconsin (USA).

112 Biogeochemical cycles and trophic levels in HAMOCC are connected by nutrient uptake
113 and remineralization of organic matter, including co-limitation by major macro and micro
114 nutrients, such as phosphate, nitrate, and dissolved iron^{52, 53}. A sediment module accounts for
115 deposition processes of solid constituents as well as for the biogeochemistry of pore water
116 tracers in the upper bioturbated sediments⁵³. Resuspension in the model configuration
117 described here is implemented after (ref. 54). Tracer transport is simulated by MPIOM.

118 The simulation has been initialized by a spin-up run of 120 years with repeated forcing
119 of the first 20 years of ERA40 data (1958-1977). River runoff is prescribed as monthly
120 climatological means, calculated by the Hydrological Discharge model⁵⁵.

121 Additional funding information

122
123
124 The acquisition and compilation of silicate data from the western Arctic was
125 supported by the Network Center of Excellence ArcticNet and Fisheries and Oceans, Canada,
126 Atlantic Zone Offshore Monitoring Program (AZOMP). The captains and the crew of *CCGS*
127 *Hudson*, chief scientists and scientific parties of AZOMP are acknowledged. The analysis of
128 silicate data from the Labrador Sea was supported by a grant from the National Sciences and
129 Engineering Research Council of Canada to the CCAR network VITALS (Ventilation and
130 Transports across the Labrador Sea).

131 The EEL is funded through UK NERC's National Capability program.

132 The nutrient analysis of the Santander standard section has been performed in
133 relationship with the project Radiales funded by the Spanish Institute of Oceanography.

134 The PAP sustained observatory work was supported through the Natural Environment
135 Research Council (NERC), UK, project Oceans 2025 and National Capability. The PAP-SO
136 and ship of opportunity in that region also contribute to the EU funded FixO3 project EU
137 312463 and the NERC Greenhouse Gas TAP NE/k00249x/1.

138 **2. Supplementary Text**

139 Validation of HAMOCC

141 The simulated silicate concentrations during April are comparable to World Ocean Atlas
142 climatology (Fig. S2). A clear separation line between subpolar and subtropical water masses
143 aligns with the North Atlantic Current and maximum concentrations are found in the
144 Labrador Sea convections site, while elevated concentrations embed the northern Irminger
145 Sea and Iceland Basin. The simulated concentrations in the Baffin Bay are, however, much
146 lower than the representation in the World Ocean Atlas. Also note that the World Ocean
147 Atlas shows highest silicate concentrations in the Irminger Sea region during March (Fig.
148 S2a), followed by maximum values in the Labrador Sea during April (Fig. 2Sb).

149 In addition, primary production is in good agreement with satellite data presented in (ref. 56),
150 with about $580 \text{ mg C m}^{-2} \text{ d}^{-1}$ in the Central Irminger Sea, $650 \text{ mg C m}^{-2} \text{ d}^{-1}$ in the Iceland
151 Basin and $750 \text{ mg C m}^{-2} \text{ d}^{-1}$ at Reykjanes Ridge during July to September 1998-2010.
152 Moreover, observed annual cycles in the Irminger Sea of near-surface nitrate concentrations
153 as well as phytoplankton and zooplankton abundances presented in (ref. 57) for the years
154 2001 and 2002 are well reproduced by the model, with winter nitrate concentrations ranging
155 between 10 and 14 μM .

156 A linear regression analysis of the simulated near-surface (0 – 150 m) March silicate at each
157 HAMOCC model grid for the period 1990-2011 reveals a significant negative trend in the
158 following regions: *i*) At the entrance to the Rockall Trough (west of the British Isles) where
159 several water masses with strongly contrasting properties meet, *ii*) along the periphery of the
160 SPG through the Iceland Basin, the Reykjanes Ridge, the Irminger Sea and the Labrador Sea,
161 *iii*) the south Iceland Shelf, *iv*) along the sub-arctic front in the Nordic Seas and *v*) in a region
162 in the central SPG, south of Greenland (Fig. S3). This is likely due to the westward retracting
163 SPG during this period¹¹, and the associated replacement of silicate rich subarctic waters with

164 silicate poorer Atlantic waters along the retracting subarctic front. A similar westward
165 retraction of the subarctic front in the Nordic Seas would also induce a silicate decline near
166 the frontal zone there. Periods with weak atmospheric forcing result in both a declining
167 SPG^{11, 12} and a westward shift of the subarctic front in the Nordic Seas⁵⁸.

168 The HAMOCC model shows very strong silicate variability in the central SPG since the late
169 1950s, which closely follows the gyre index from (ref. 11), based on output from the Miami
170 Isopycnal Coordinate Ocean Model (MICOM) (Fig. S4). The negative trend in the central
171 SPG (54-56°N, 48-45°W, blue blob south of Greenland in Fig. S3) is primarily caused by an
172 extreme drop of nearly 6 μM during the years 1995-1999, when the gyre suddenly declined¹¹.

173 HAMOCC, however, does not show a significant decline along the WOCE line ARW7 (Fig.
174 S3) where the observations show a clear silicate decrease (Fig. 2 and Table 1). It is well
175 known that such model systems can produce realistic temporal variability associated with
176 deep convection, but they seldom correctly identify the location of real convection regions.
177 The general circulation model MPIOM, which is the physical component of HAMOCC, has
178 such limitations, and this could explain the likely spurious spatial pattern within the central
179 SPG.

180

181 Arctic silicate flux estimate

182

183 Since 1997, the Arctic system has been under the influence of an anticyclonic circulation
184 regime, described as a positive phase of the Arctic Ocean Oscillation²⁶. Under these
185 conditions, wind forcing leads to freshwater (FW) accumulation in the Arctic Ocean through
186 Ekman convergence and thus a reduction of the FW flux to the North Atlantic subpolar
187 regions (Fig. S7b). Most of the FW accumulation occurs in the Beaufort Gyre, where not only
188 Pacific Water (PW) rich in silica accumulates, but also FW from river runoff⁵⁹ with even
189 higher silicate concentrations⁶⁰ converges. Estimates of the FW build up in the Beaufort Gyre
190 since the mid-1990s range between 8,000 km³ and 12,000 km³ (refs. 28, 61). Knowing the
191 silicate concentrations representative of this FW enables us to estimate the associated
192 reduction in Arctic silicate flux to the subpolar North Atlantic Ocean.

193 *Silicate concentration representative of the FW accumulated in the Beaufort Gyre.*

194 Estimations of FW accumulation in the Arctic are made with respect to the 34.8
195 isohaline, typically located within the upper 350 m depth in the Canada Basin. Above it (50-
196 250 m depths), a silicate maximum ($\sim 35 \mu\text{M}$) is observed, associated with the PW (e.g. Fig. 7
197 in ref. 9). The PW halocline is found between the PW core and the 34.8 isohaline, with lower
198 but still high silicate concentrations.

199 On its way from the Canada Basin through the Canadian Arctic Archipelago to Davis
200 Strait, homogenization of the Pacific-origin waters occurs as noted by (ref. 8). Similar total
201 levels of salt and silicate are found in the upper 150 m for Silicate-Rich Arctic Water (SRAW)
202 in Baffin Bay and the Canada Basin. Thus, the silicate concentration in the homogenized
203 SRAW ($\sim 22 \mu\text{M}$)⁸ is assumed to be representative of the Pacific-origin waters in the Canada
204 Basin. In order to estimate the silicate accumulation in the Beaufort Gyre ($\sum \text{Si}_{\text{BG}}$), a reference
205 silicate concentration, here represented by the mean concentration of the Arctic, must be
206 subtracted from the SRAW concentration. Using the Pangaea data set
207 (<https://www.pangaea.de/>), we get $\text{Si}_{\text{ref}} \sim 11 \mu\text{M}$. This gives:

208

209 $\sum Si_{BG(I)} = FW_{BG} [8000-12000 \text{ km}^3] \cdot (22 \text{ } \mu\text{M} - 11 \text{ } \mu\text{M})$
 210 $= -[8.8-13.2] \cdot 10^{16} \text{ } \mu\text{mol}$

211

212 Alternatively, we could estimate $\sum Si_{BG}$ from the silicate maximum of the PW,
 213 previously estimated to contribute 50% to the total FW content in the Beaufort Gyre⁶².

214

215 $\sum Si_{BG(II)} = 0.5 \cdot FW_{BG} [8000-12000 \text{ km}^3] \cdot (35 \text{ } \mu\text{M} - 11 \text{ } \mu\text{M})$
 216 $= -[9.6-14.4] \cdot 10^{16} \text{ } \mu\text{mol}$

217

218

219 *Contribution to the subpolar North Atlantic.*

220 According to (ref. 9), between 85 and 100% of the silicate in the Arctic leaves the basin
 221 through the Canadian Arctic Archipelago, mainly in the density range $\sigma_\theta = 27.0 - 27.5$. Based
 222 on the climatological distribution of the 27.0 and 27.5 isopycnals in the North Atlantic
 223 (including the Labrador and Irminger seas), we estimate the volume into which the SRAW
 224 potentially would redistribute: $V_{NAII} = 4.11 \cdot 10^{14} \text{ m}^3$.

225 The silicate decrease in the subpolar North Atlantic, caused by the retention of silicate in
 226 the Arctic Ocean (assuming that 90% reaches the North Atlantic) is therefore:

227

228 $\Delta Si_{NAII} (I) = 0.90 \cdot \sum Si_{BG(I)} / V_{NAII} = -0.90 \cdot [8.8-13.2] \cdot 10^{16} \text{ } \mu\text{mol} / 4.11 \cdot 10^{14} \text{ m}^3$
 229 $= -(0.19-0.29) \text{ } \mu\text{M}$

230

231 $\Delta Si_{NAII} (II) = 0.90 \cdot \sum Si_{BG(II)} / V_{NAII} = -0.90 \cdot [9.6-14.4] \cdot 10^{16} \text{ } \mu\text{mol} / 4.11 \cdot 10^{14} \text{ m}^3$
 232 $= -(0.21-0.33) \text{ } \mu\text{M}$

233

234 Thus, the accumulation of SRAW in the Beaufort Gyre and Canada Basin could explain
 235 up to 10-20% of the total silicate decline observed in the subpolar North Atlantic (1.5-2 μM).
 236 A more realistic estimate must, however, include changes in FW transport into the Arctic
 237 through the Bering Strait.

238

239 *FW transports through Bering Strait.*

240 The annual FW transport through the Bering Strait has increased from 2000–2500 km^3 in
 241 2001 to 3000-3500 km^3 in 2011²⁹. Assuming a linear increase as observed in ref. 29 (100 km^3
 242 per year over ten years), this would result in a FW increase of 5000 km^3 from 2001 to 2011,
 243 which is about half of the observed FW accumulated in the Beaufort Gyre.

244 On the other hand, a 26% decrease in the FW transport through Davis Strait from 4500 \pm
 245 730 km^3 for the period 1987-1990 to 3300 \pm 220 km^3 for the period 2004-2010 would explain
 246 up to 10,000 km^3 of FW accumulation in the Arctic⁵². Together, they would result in a FW
 247 accumulation of 15,000 km^3 , ~1/3 contribution from Bering Strait FW transports and ~2/3
 248 from Davis Strait FW transports.

249 Thus accounting for the increased Bering Strait FW contribution to the observed
 250 Beaufort Gyre FW accumulation since the mid-1990s, we estimate the Arctic contribution to
 251 the North Atlantic silicate decline (1.5-2 μM , Fig. 2a) to be less than 15%.

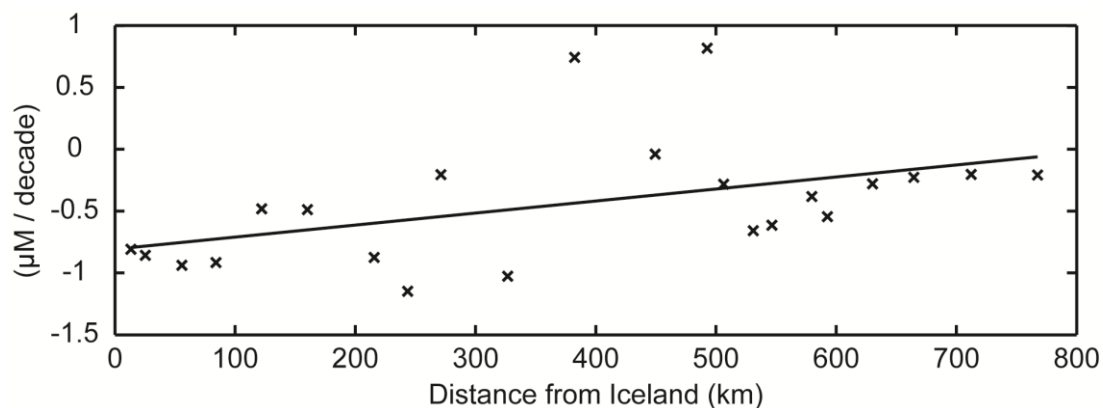
252

253

254

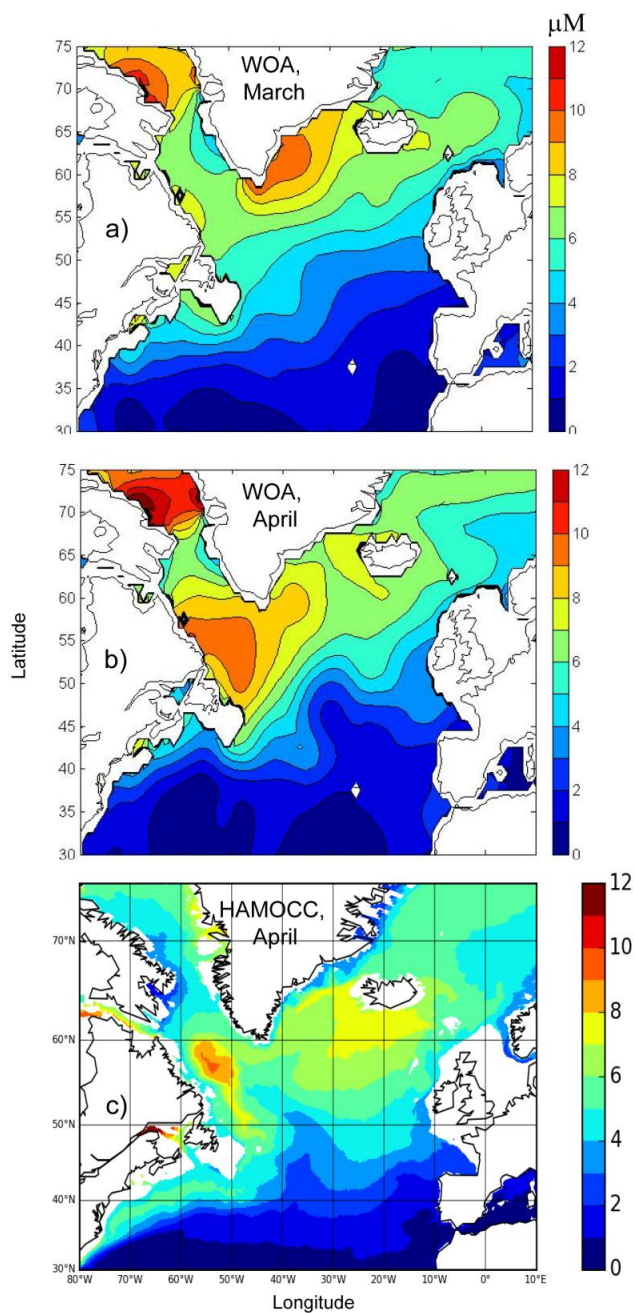
255 **3. Supplementary Figures**

256



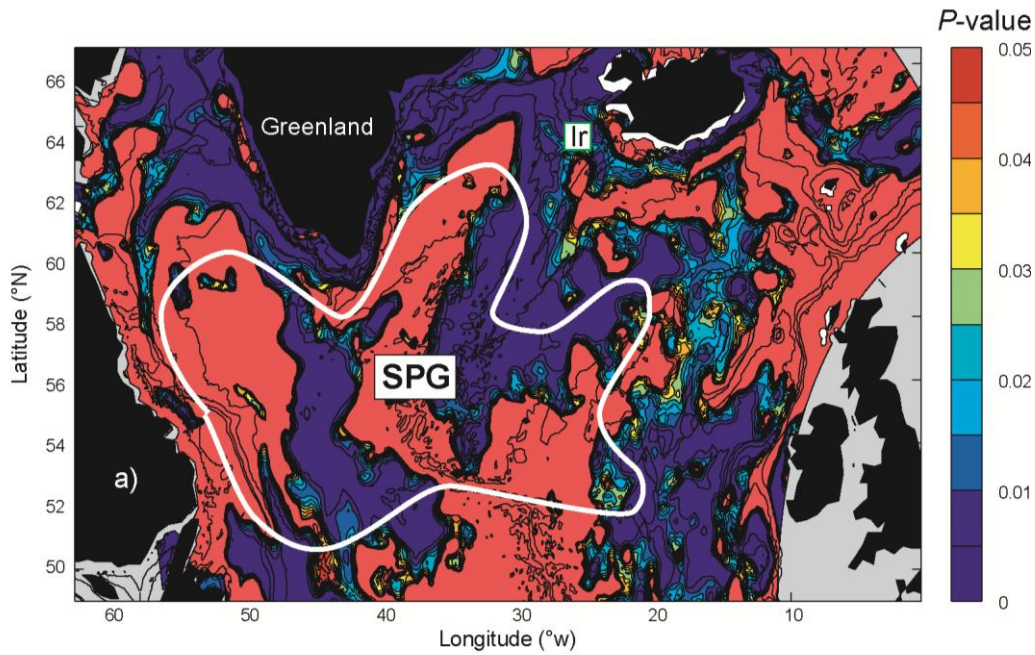
257

258 **Fig. S1** Rate of change in silicate concentrations between 150-600 m from 1997 to 2015 for
259 each EEL station between Iceland (0 km) and Rockall (800 km) (see Fig. 4). Only stations
260 where data from more than five cruises are available have been included. The rate of change
261 has been calculated by a least square analysis.



263

264 **Fig. S2 Climatological upper-ocean (average over 0-200 m) silicate concentrations.**
 265 Panels a) and b) show the representation in the World Ocean Atlas (WOA²⁰) for March and
 266 April, respectively and c) shows the simulated values from HAMOCC for April (1960-2012).
 267 The figure was produced using the softwares Matlab R2013b, (<https://www.mathworks.com>)
 268 (panels a) and b) and the Python programming language (Python Software Foundation.
 269 Python Language Reference, version 2.7, available at <http://www.python.org>).

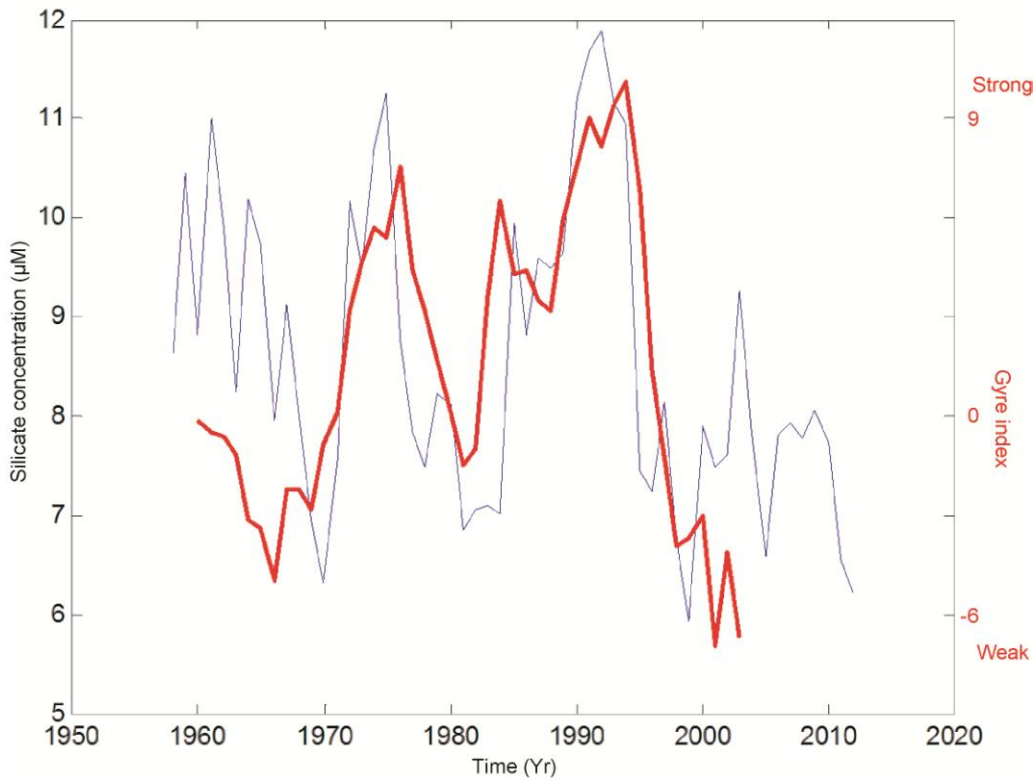


270

271 **Fig. S3 Linear trend in the simulated (HAMOCC) near-surface (0 – 150 m) silicate**
 272 **during March.** The colors show *P*-values from a linear regression analysis of the silicate at
 273 each model grid for the period 1990-2011. The blue colors represent the regions where a
 274 declining trend is simulated, and the areas colored red show no clear trend. The rough outline
 275 of the subpolar gyre (SPG) is depicted with the white curve. The figure was produced using
 276 the software Matlab R2013b, (<https://www.mathworks.com>).

277

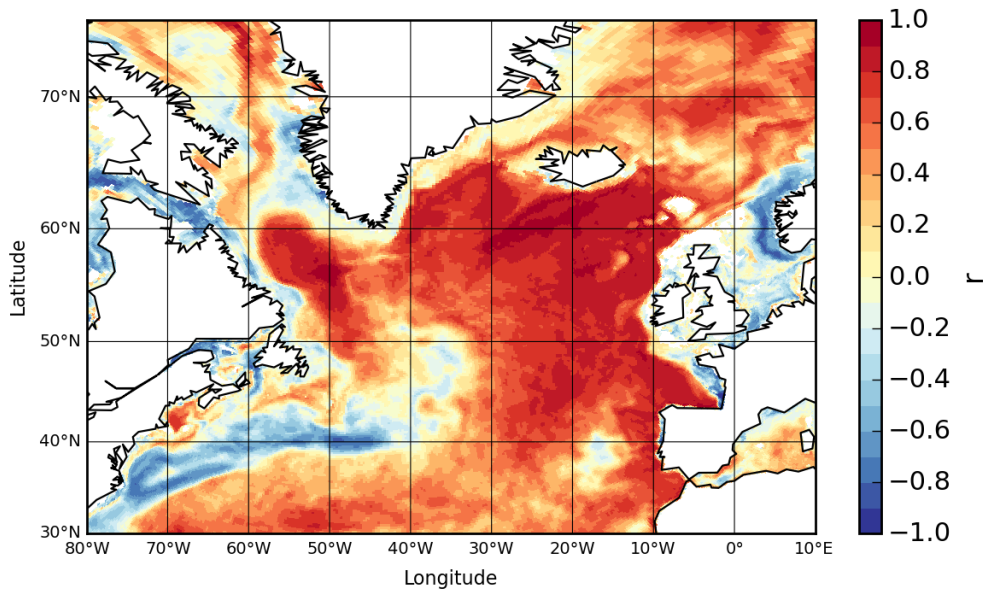
278



279

280

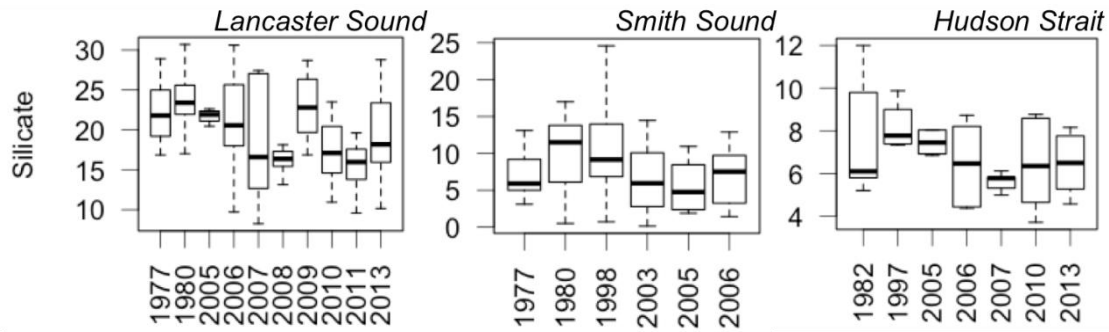
281 **Fig. S4** Simulated near-surface (0-200 m) March silicate concentration (HAMOCC) in the
 282 central SPG (54-56°N, 48-45°W) and the gyre index presented by (ref. 11) (red), which was
 283 based on the Miami Isopycnal Coordinate Ocean Model (MICOM).



284

285 **Fig. S5** Correlations between the simulated winter (DJF) near-surface silicate
 286 concentrations, and the mixed layer depth (DJF) at every model (HAMOCC) grid-point
 287 for the years from 1958 to 2012. The figure was produced using the Python programming
 288 language (Python Software Foundation. Python Language Reference, version 2.7, available at
 289 <http://www.python.org>).

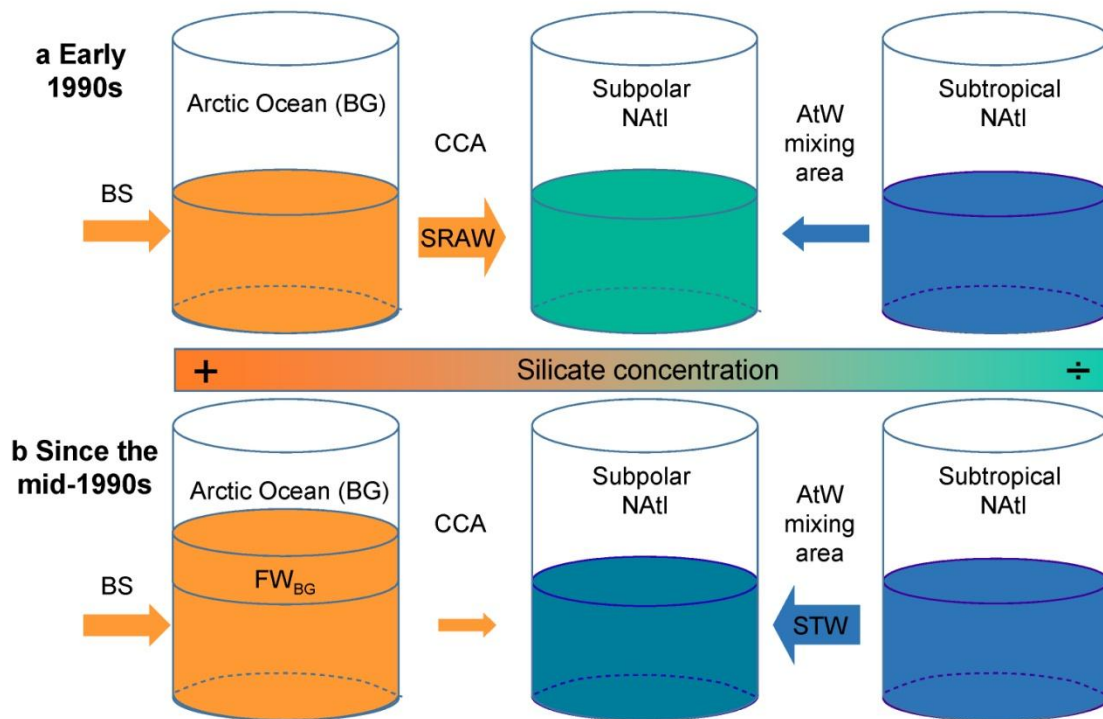
290
291



292

293 **Fig. S6.** Temporal changes of the silicate concentration (μM) in the Arctic Outflow at three
294 passages through the Canadian Arctic Archipelago: Lancaster Sound (50-150 m), Smith
295 Sound (0-100 m) and Hudson Strait (50-150 m).

296



297

298 **Fig. S7. Schematic diagram of Silicate-Rich Arctic Water (SRAW) and subtropical**
299 **Water (STW) contributions to the silicate content in the subpolar North Atlantic. a)** The
300 situation at the beginning of the 1990s, after the large loss of Arctic Freshwater content and
301 before the beginning of large fresh water accumulation in the Beaufort Gyre (BG) since the
302 mid-1990s. **b)** After the mid-1990s, with SRAW of Pacific origin accumulation in the BG
303 (FW_{BG}) through Ekman convergence and reduction of SRAW flux to the North Atlantic
304 Subpolar regions. BS, Bering Strait; CAA, Canadian Arctic Archipelago.

305